photonics

MDPI

Article

Joint Pre- and Post-Equalization with Higher-Order Modulation Formats in SDM-Based Optical MIMO Systems

Jasmeet Singh [1,2,*], Andreas Ahrens [1] and Steffen Lochmann [1]

[1] Department of Electrical Engineering and Computer Science, Hochschule Wismar, Philipp-Müller-Straße 14, 23966 Wismar, Germany
[2] ETSIST, Universidad Politécnica de Madrid, Campus Sur, Calle Nikola Tesla s/n, 28031 Madrid, Spain
* Correspondence: jasmeet.singh@hs-wismar.de

Abstract: The multiple-input and multiple-output (MIMO) technology is a promising area of research to cope up with the demands of higher data rates and capacity. In the optical communication domain, the combination of space-division multiplexing (SDM) with higher-order modulation (HOM) formats over an optical MIMO system actively addresses these challenges. By allowing multi-level signaling with limited increment in the transmitter's complexity, a jointly designed pre- and post-equalization (PPE) for an optical MIMO system with a multi-mode fiber (MMF) link is proposed. Cost-effectiveness of the system is incorporated by utilizing intensity modulation/direct detection (IM/DD) with HOM formats such as pulse-amplitude modulation (PAM) schemes. With the aid of a numerical optimization algorithm, the proposed joint-PPE filter coefficients are optimized with respect to the MMF channel and the transmit power constraint. In contrast to existing research on the single-mode fiber (SMF) based optical systems, the effectiveness of the proposed joint-PPE filter is analyzed on an MMF link, which is considerably degraded by the modal dispersion. In the analyzed experimental scenario, the proposed joint-PPE scheme confirms to be beneficial as compared to the post-equalization only (PE-only) in terms of bit-error rate (BER) performance. Furthermore, the required average received optical power to reach a BER 10^{-4} by the joint-PPE scheme is improved by 2 dB with comparison to the minimum mean-squared error (MMSE) PE-only.

Keywords: multi-mode fiber; optical MIMO; optical fiber transmission

Citation: Singh, J.; Ahrens, A.; Lochmann, S. Joint Pre- and Post-Equalization with Higher-Order Modulation Formats in SDM-Based Optical MIMO Systems. *Photonics* **2022**, *9*, 876. https://doi.org/10.3390/photonics9110876

Received: 4 October 2022
Accepted: 16 November 2022
Published: 19 November 2022

1. Introduction

With the new trends in technology such as cloud computing, Internet of Things and 5G fronthaul, the capacity of optical systems based on single-mode fiber (SMF) transmission links has reached their limit [1]. Hence, the development of cutting-edge communication links, which subjects to address the incessant demand for higher data capacity and cost-effectiveness, is crucially required. By utilizing the transverse spatial extent of a multi-mode fiber (MMF) core, parallel individual data channels can be created over non-overlapping subsets of excited mode groups [2]. This approach is named as space-division multiplexing (SDM) in which an MMF is essential, as these fibers support up to 100 transverse spatial modes that can be translated as parallel data channels [1,2]. SDM also provides the higher spectral efficiency to cope up with the bandwidth-intense applications. The capacity crunch due to the SMFs is eliminated by using the MMFs with SDM. Moreover, for short reach optical links, intensity modulation/direct detection (IM/DD) systems with an MMF provides a cost-effective solution.

The consequences of employing the MMFs are mode scrambling and inherent inter-modal dispersion, which are limiting factors for the maximum achievable data rates [3]. By applying multiple-input and multiple-output (MIMO) techniques, the adverse effects of the mode scrambling are mitigated and higher data capacity is achieved [4–6]. Additionally, the higher spectral efficiency can be boosted by utilizing higher-order modulation

(HOM) formats which include pulse-amplitude modulation (PAM) schemes. These HOM formats, PAM-M, provide larger constellation sizes, $M > 2$, which offer efficient use of the bandwidth. The main challenges are to excite a particular mode group and extraction of them at the receiver due to strong temporal broadening of the light from the MMF channel. The countermeasures to mitigate the dispersive-induced impairments are by using the physical optical components such as dispersion-shifted fibers or fiber Bragg gratings [7]. Most prevalent dispersion compensation mechanisms include the use of digital signal processing such as equalization.

Conventionally, when the trade-off between cost-effectiveness and complexity is taken into account, a linear MIMO equalizer is preferred. The non-linear equalizers, such as Viterbi equalizer or Tomlinson–Harishima precoder, perform better than a linear equalizer such as minimum mean-squared error (MMSE). However, the mathematical traceability and comprehensive implementation of a linear equalizer is chosen in comparison to the complex realization of the non-linear equalizer [1,8]. From the literature, it is evident that the equalizer present at both the transmitter and the receiver offers better performance than the equalization which is only limited to either the transmitter or the receiver [9,10]. Few studies have explored the usefulness of pre- and post-equalization (PPE) schemes, and these schemes have been tested on optical systems based on SMF, which is impaired with chromatic dispersion only [11–13]. The joint design and optimization of a PPE filter with HOM formats for an MMF-based optical MIMO system has not been established yet.

Against this background, the novelty of this work is improvement in the bit-error rate (BER) using the joint-PPE scheme while employing HOM formats in an IM/DD system. The competency of the joint-PPE scheme is provided over an optical (2×2) MIMO system based on an MMF channel, which is critically impaired with inter-symbol interference (ISI) and inter-channel interference (ICI). The coefficients of the PPE are mutually computed and optimized using a numerical optimization algorithm in presence of the frequency-selective channel. This work also provides a cost-effective and low complexity solution by using a parallel frame synchronization (PFS) experimental setup. Finally, the performance benefits from the multi-level signaling with joint-PPE scheme are validated and compared with MMSE based post-equalization only (PE-only) with the help of an experimental setup.

2. System Model

The spectral efficiency of the transmission link is improved by integrating the MIMO signal processing technique with HOM formats in the optical domain. In this work, a (2×2) MIMO technique with an optical MMF link is implemented, and the corresponding system model is provided in Figure 1. This given optical MIMO transmission system model consists of two MIMO outputs n_{R} and two MIMO inputs n_{T}, which are described as $(n_{\mathrm{R}} \times n_{\mathrm{T}})$. This model also incorporates the joint-PPE filter using an MMF channel with the PFS. The serial input data symbol $s(k)$ is the result of concatenation of two distinct data frames D1 and D2 from two MIMO inputs $s_\mu(k)$, respectively, with $\mu = 1, \ldots, n_{\mathrm{T}}$ and $s(k) = \begin{pmatrix} s_1(k) & s_2(k) \ldots s_\mu(k) \end{pmatrix}$, where $k \in \mathbb{N}$. Moreover, the symbol amplitudes $s_\mu(k)$ at the μ-th data frames are defined as $s_\mu(k) \in \{s_{\mu,0}, \ldots, s_{\mu,M-1}\}$, with $k \in \mathbb{N}$ and k represents a discrete-time index. With the help of Gray coding, each symbol in $s_\mu(k)$ is mapped to a PAM-M format, where M represents the constellation size. Overall, the functionalities of the MIMO transmitter include the concatenation of different frames into $s(k)$, pre-equalizer $p(k)$ implementation and serial to parallel conversion of pre-equalizer signal $b(k)$, where $b(k) = \begin{pmatrix} b_1(k) & b_2(k) \cdots b_\mu(k) \end{pmatrix}$. One of the crucial components of the joint-PPE scheme is a pre-equalizer, which is characterized as a linear finite impulse response (FIR) filter. Consequently, $s_\mu(k)$ undergoes pre-equalization, which results in generation of multi-level signals that are denoted as $b_\mu(k)$ at the μ-th input. The number of distinct amplitude levels N of $b_\mu(k)$ is calculated as $L_{\mathrm{p}} = \log_2(N)$ with L_{p} corresponding to the number of the pre-equalizer filter taps. The pre-equalized multi-level signal is defined as $b_\mu(k) = \{b_{\mu,0}, b_{\mu,1}, \ldots, b_{\mu,N-1}\}$. The purpose of the pre-equalizer is to mitigate the adverse effects of ISI and ICI based on the estimated channel. Please note that prior to the

transmission, the transmit power of the symbols with the highest amplitude at both MIMO inputs is restricted with respect to the maximum optical power $P_{\mathrm{s},\mu}^{(\max)}$ of the provided laser sources. This relation is analytically defined as

$$s_{\mu,M-1} = b_{\mu,N-1} = \mathrm{q} \cdot P_{\mathrm{s},\mu}^{(\max)} \quad , \tag{1}$$

with q denoting the conversion factor from electrical to optical domain. While implementing HOM formats with multi-level signaling, the peak-to-average power ratio is held constant by using (1). After this power limitation, the multi-level signals $b_\mu(k)$ are propagated across an MMF channel $h_{\nu\mu}(k)$, where $\nu = 1, \ldots, n_{\mathrm{R}}$. The concept of MIMO technique is accomplished by using centric and eccentric light launching conditions using SDM, as demonstrated in Figure 2. Using the transverse spatial extent of an MMF, different mode groups of light are excited, which propagate in the fiber with distinct speeds. In Figure 2, the light is launched at the center of the optical fiber for the first MIMO input Tx_1, which results in excitation of lower-order modes. Moreover, the higher-order modes are excited at the second MIMO input Tx_2 with eccentric launching of the light using a 15 µm offset [14,15].

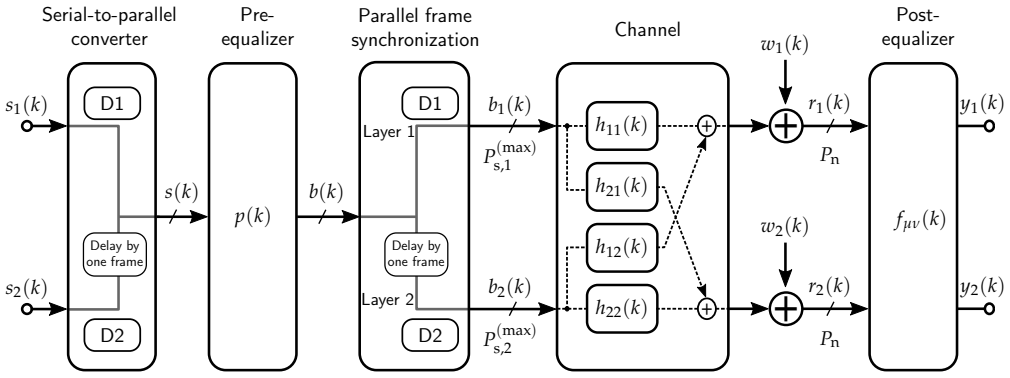

Figure 1. Electrical (2 × 2) MIMO system model with jointly designed pre- and post-equalization filter.

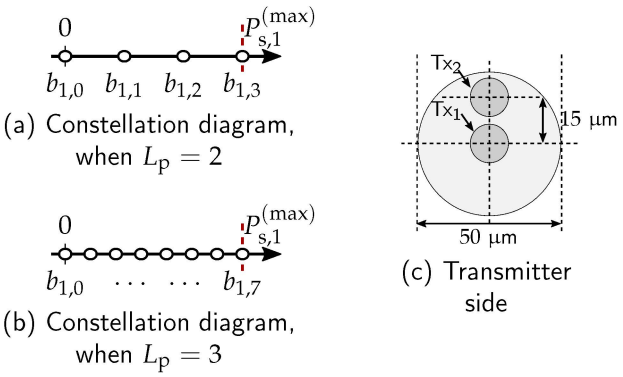

Figure 2. Illustrating the multi-level signals after pre-equalization using PAM-2 configuration, where: (**a**) $L_{\mathrm{p}} = 2$; and (**b**) $L_{\mathrm{p}} = 3$. At the transmitter, the light launching conditions into the optical fiber core are included in (**c**), which represents the centric 0 µm and eccentric 15 µm light launching conditions for two MIMO inputs Tx_1 and Tx_2, respectively.

Thereafter, the transmitted signal $b_\mu(k)$ is degraded by the ISI and ICI due to the MMF channel. The frequency-selective behavior of the channel $h_{\nu\mu}(k), \forall\, \nu, \mu$ produces the ISI. The independent data channels, which are created using SDM, are not ideally orthogonal. Hence, it results in the ICI, $h_{\nu\mu}(k)$ with $\nu \neq \mu$. After the channel, the signal suffers from

additive, white and Gaussian noise (AWGN) [15]. The mathematical description of the provided system model in matrix notation is derived as

$$\boldsymbol{r} = \boldsymbol{H} \cdot \boldsymbol{P} \cdot \boldsymbol{s} + \boldsymbol{w} \ , \tag{2}$$

where $\boldsymbol{r}$ is the received signal matrix, and $\boldsymbol{H}$ is the channel matrix including direct and cross-talk components. The pre-equalizer and transmitted symbols are denoted by $\boldsymbol{P}$ and $\boldsymbol{s}$, respectively. The AWG noise is considered to be $\boldsymbol{w}$ in (2). Finally, the received signal $\boldsymbol{r}$ undergoes the post-equalization $\boldsymbol{F}$. The output signal matrix $\boldsymbol{y}$ is defined as

$$\begin{aligned} \boldsymbol{y} &= \boldsymbol{F} \cdot \boldsymbol{r} \\ \boldsymbol{y} &= \underbrace{\boldsymbol{F} \cdot \boldsymbol{H} \cdot \boldsymbol{P}}_{\text{Term 1}} \cdot \boldsymbol{s} + \underbrace{\boldsymbol{F} \cdot \boldsymbol{w}}_{\text{Term 2}} \ . \end{aligned} \tag{3}$$

From (3), Term 1 emphases that the pre- and post-equalizers can jointly contribute to recover the transmitted data by mitigating the effect of the channel. Secondly, Term 2 highlights the contribution of the post-equalization in the noise amplification, which will result in a performance degradation. While considering that the ISI and ICI are completely mitigated with the help of pre-equalizer and post-equalizer, (3) is condensed further as follows

$$\begin{aligned} \boldsymbol{F} \cdot \boldsymbol{H} \cdot \boldsymbol{P} &= \boldsymbol{I} \\ \boldsymbol{y} &= \boldsymbol{s} + \boldsymbol{F} \cdot \boldsymbol{w} \ , \end{aligned} \tag{4}$$

with $\boldsymbol{I}$ denoting the identity matrix. It is clear that the post-equalization is responsible for noise enhancement at the receiver. Therefore, the hypothesis implies that by shifting the equalization efforts to the transmitter will reduce the noise amplification and will compensate the channel interferences. Consequently, the system performance can be improved. The noise amplification due to the presence of the post-equalizer is quantified using the noise power $\widetilde{P}_{\mathrm{n},\mu}$. The expression is provided as follows

$$\widetilde{P}_{\mathrm{n},\mu} = \theta_\mu \cdot P_{\mathrm{n}}, \qquad \theta_\mu = \sum_{\nu=1}^{n_{\mathrm{R}}} \sum_{k=0}^{L_{\mathrm{f}}-1} |f_{\mu\nu}[k]|^2 \ , \tag{5}$$

where the noise weighting factor θ_μ is derived from the amplitude of the post-equalization coefficients $f_{\mu\nu}[k]$. Prior to the post-equalization, the noise power is denoted as P_{n}. Furthermore, L_{f} defines the length of the post-equalization filter. From (5), a direct relation between the post-equalization coefficients and the noise enhancement is established. In order to evaluate the performance of the provided (2×2) optical MIMO system, the key performance indicator is considered as BER $P_{\mathrm{BER}}^{(\mu)}$ of μ-th layer, and it is defined as

$$\begin{aligned} P_{\mathrm{BER}}^{(\mu)} &= \frac{1}{\log_2(M_\mu)} \left(\frac{M_\mu - 1}{M_\mu} \right) \operatorname{erfc}\left(\sqrt{\frac{\varrho_\mu}{2}} \right), \\ \text{where,} \quad \varrho_\mu &= \frac{U_{\mathrm{A},\mu}^2}{\widetilde{P}_{\mathrm{n},\mu}} = \frac{U_{\mathrm{A},\mu}^2}{\theta_\mu \, P_{\mathrm{n}}} \ , \end{aligned} \tag{6}$$

with $\operatorname{erfc}(\cdot)$ denoting the complementary error function. In (6), at the μ-th input, M_μ defines the size of the constellation, the signal-to-noise-ratio (SNR) is ϱ_μ and the half-vertical eye-opening is $U_{\mathrm{A},\mu}$. It is worth noting that (6) is only valid when the ICI and the ISI occurring are entirely removed. From (5) and (6), it is evident that the post-equalization coefficients are degrading the performance of the system in terms of BER.

Therefore, the prime objectives of the jointly designed PPE filter are minimal noise enhancement and BER improvements while restraining the transmitter's complexity. Hence, a few-tap pre-equalizer is recommended, which aims to improve the system performance by shifting a few equalization efforts from the receiver to the transmitter.

3. Pre- and Post-Equalizer

According to the literature, a segregated design of the pre- and post-equalizer is mainly practiced. The computation of the pre-equalizer coefficients is based on the zero-forcing principle. In contrast, this work is concentrated on jointly designing and optimizing the pre- and post-equalizer. Moreover, the multi-level signals, which are produced by the pre-equalizer, target to partially compensate the channel interferences, especially the cross-talk from the adjacent channel. The concept of the joint-PPE scheme is to improve the system BER by shifting a few equalization efforts to the transmitter, while considering the power constraint and minimal surge in the transmitter complexity.

The pre-equalizer is characterized as a linear FIR filter with a given length of L_p, and it is defined as

$$b_\mu(k) = \sum_{i=1}^{L_\mathrm{p}} p_{i,\mu} \cdot s[k-(i-1)], \qquad \mu = 1, \ldots, n_\mathrm{T} \ , \tag{7}$$

with $p_{i,\mu}$ representing the pre-equalizer coefficient at i-th instance at the μ-th input. As the input signal $s(k)$ consists of concatenated frames from both the MIMO inputs, the pre-equalizer is applied to $s(k)$ instead of executing the pre-equalization separately to the individual MIMO inputs. When the identical pre-equalizer coefficients are implemented on both layers, the marginal increase in the transmitter's complexity is advantageous. Moreover, the elimination of cross-talk is primarily targeted. The graphical representation of the constellation diagram with multiple levels is demonstrated in Figure 2. Prior to the transmission, the PAM-2 modulated signal undergoes the pre-equalization with $L_\mathrm{p} = 2$ in (a) and $L_\mathrm{p} = 3$ in (b), resulting in generation of the multi-level signaling. Additionally, the power constraint for the first layer is also depicted in Figure 2.

The joint-PPE filter is calculated using an interior-point optimization algorithm, which is subjected to constraints [16]. The optimization problem is tailored as follows

$$\begin{aligned} &\underset{p(k),\, f_{\mu\nu}(k)}{\text{minimize}} && \theta_\mu(h_{\nu\mu}(k)) && \nu = 1, \ldots, n_\mathrm{R} \\ &\text{subject to} && f_{\mu\nu}(k) * h_{\nu\mu}(k) * p(k) \approx z_\nu(k), && \forall \nu \\ &\text{and} && s_{\mu,M-1} = b_{\mu,N-1} = \mathrm{q} \cdot P_{\mathrm{s},\mu}^{(\max)} \ , \end{aligned} \tag{8}$$

where $*$ refers to the convolution operator, and $z_\nu(k)$ is the approximation of the PPE filter with the Nyquist filter. The prime goal of (8) is to encounter the ISI first and consequently, deal with the ICI. The suggested length of the pre-equalizer is restricted to two or four taps because a minimal increase in the transmitter complexity is essential.

From (8), it is clear that an accurate channel estimate is required in order to compute the joint-PPE coefficients. Additionally, the amplitude of the joint-PPE coefficients is constrained by the maximum output power of the laser source.

4. Simulation Results

The benefits of the joint-PPE schemes are estimated by using a Monte Carlo simulation. A (2×2) MIMO system, as illustrated in Figure 1, with a 100 m long MMF is considered for the simulation. There are three sequential steps, which are conducted to evaluate the performance of the proposed joint-PPE scheme. In the first step, an MMSE post-equalization is implemented while considering the pre-equalizer as a Dirac delta function. The channel state information is computed in the second step by using a pilot-based least square estimator algorithm. In the last step, the pre-and post-equalization filter taps are designed and optimized using the optimization algorithm in (8). Finally, the joint-PPE filter is incorporated with the provided system model and the calculated channel state information. The measured channel impulse response of a 100 m long MMF is demonstrated in Figure 3. The cross-talk $h_{12}[k]$ from the first layer to the second layer, as shown in Figure 3, is significant compared to $h_{21}[k]$. Hence, the performance of the first layer is worse than the second layer due to the substantial modal dispersion in MMF. Moreover, the proposed

hypothesis of this work targets the effective mitigation of this ICI and ISI by joint-PPE filter with minimal increase in the noise amplification.

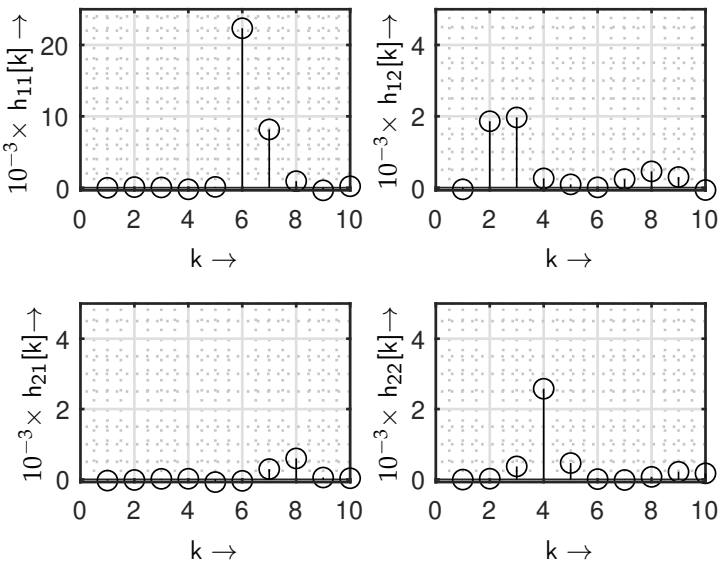

Figure 3. Measured channel impulse response of a 100 m long MMF with respect to the symbol rate $f_T = 1/T_s = 2.5$ GHz at an operating wavelength of 1550 nm.

The simulation results are analyzed with two different scenarios, depending upon the utilized modulation format on both MIMO inputs. The first scenario employs a PAM-2 scheme on both MIMO inputs. Additionally, the second scenario uses the PAM-4 format on both MIMO inputs. While using the parameters mentioned above, the Monte Carlo simulations are conducted for both scenarios, and the BER is considered the key performance indicator. For the first scenario, the layer-wise and overall BERs dependent upon SNR are illustrated in Figure 4. It is evident that the joint-PPE scheme with four pre-equalizer filter taps with PAM-2 yields a better BER performance by 2.25 dB at 10^{-4} BER compared to the PE-only with an MMSE principle. Moreover, the joint-PPE schemes significantly improve the performance of the first layer, which implies that the ICI and ISI are mitigated. Figure 5 shows the BER results for the second scenario, using PAM-4 on both MIMO inputs. In the second scenario, the joint-PPE with two-tap and four-tap pre-equalizer performs better than the MMSE-based PE-only. The noise amplification using PE-only is reduced by shifting the equalization taps from the receiver to the transmitter and jointly designing the PPE filter. The SNR gain of 1.90 dB at BER of 10^{-4} is confirmed by using the joint-PPE with $L_p = 4$ in the second scenario. When a comparison between the pre-equalizer with two and four taps is explored with PAM-4 format, an SNR gain of 0.60 dB is noted. It implies a slight improvement in the system performance. Therefore, in the analyzed case, when a trade-off between complexity and system performance is considered, a pre-equalizer with two taps should be preferred as it displays nearly similar performance benefits compared to a pre-equalizer with four taps. A detailed description of the SNR gains is depicted in Table 1.

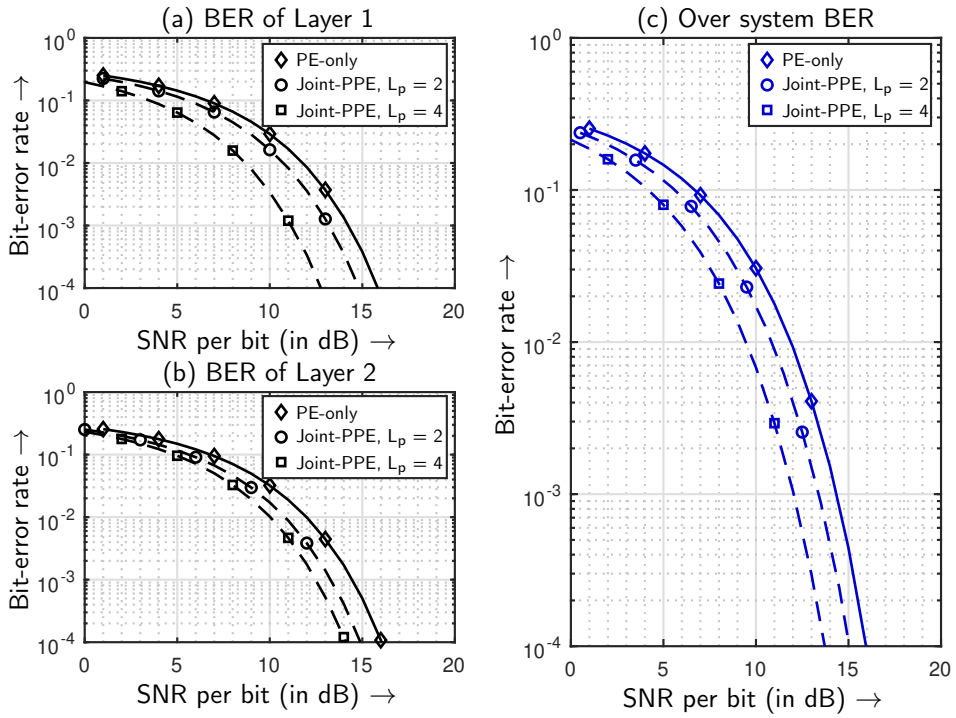

Figure 4. BER in dependent on SNR for the first scenario, where PAM-2 is utilized on both the MIMO inputs. The BER associated with PE-only and the proposed joint-PPE schemes are represented with solid and dashed lines, respectively.

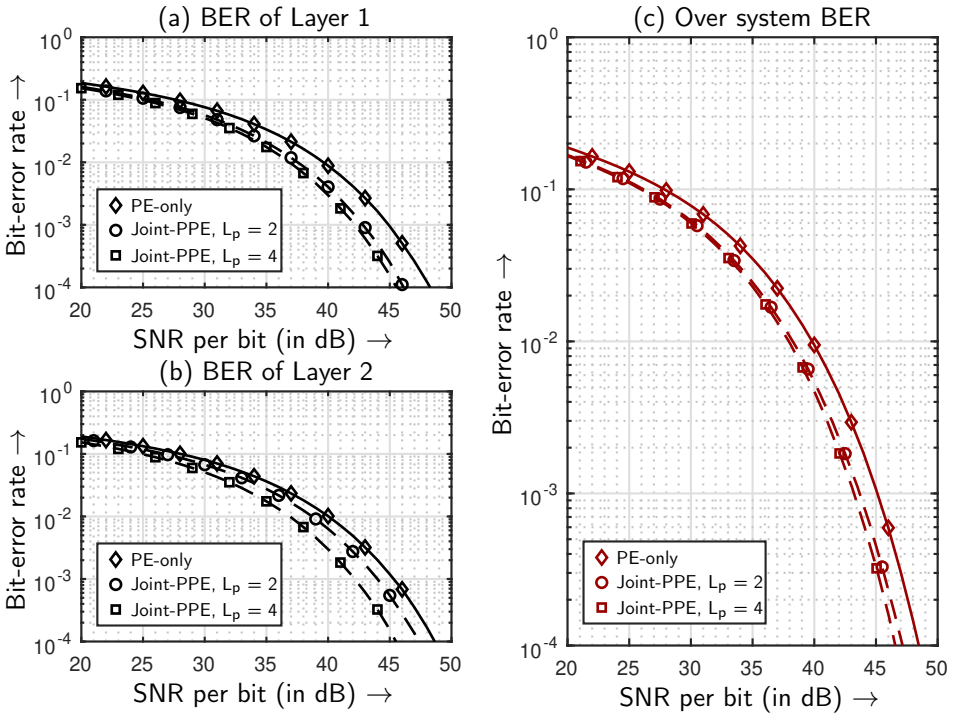

Figure 5. BER in dependent on SNR for the second scenario, where PAM-4 is utilized on both the MIMO inputs. The BER associated with PE-only and the proposed joint-PPE schemes are represented with solid and dashed lines, respectively.

Table 1. Simulated SNR gain of the (2×2) optical MIMO system at 10^{-4} BER using a 100 m long MMF channel.

Scenario	Modulation Format	Equalization	L_p	L_f	SNR (in dB) at BER of 10^{-4}	SNR Gain (in dB)
First scenario	PAM-2	PE-only	-	25	15.95	-
		Joint-PPE	2	23	15.05	0.90
			4	21	13.70	2.25
Second scenario	PAM-4	PE-only	-	25	48.50	-
		Joint-PPE	2	23	47.20	1.30
			4	21	46.60	1.90

In summary, the simulated results demonstrate the usefulness of the proposed joint-PPE filter. It signifies that the performance benefits are yielded due to adequate compensation of the interferences with minimal noise amplification. Therefore, the simulated results confirm the stated hypothesis. Moreover, these results are validated with an experimental setup provided in the following section.

5. Experimental Results

The performance benefits of the joint-PPE scheme are evaluated using an IM/DD based (2×2) optical MIMO system using an MMF channel. A picture of the experimental measurement setup is demonstrated in Figure 6, where the design of the PFS configuration is shown with the delay line. The experimental setup is constructed with the aid of the provided system model, and it is illustrated in Figure 7. The procedure for the performance evaluation of the joint-PPE schemes starts by applying PE-only using an MMSE post-equalizer. Simultaneously, the pilot symbols are appended to the transmitted data intending to estimate the channel state information. Afterwards, the joint-PPE filter coefficients are computed and optimized using the abovementioned constrained optimization algorithm. Finally, the comparison between the joint-PPE and PE-only in terms of the BER is conducted.

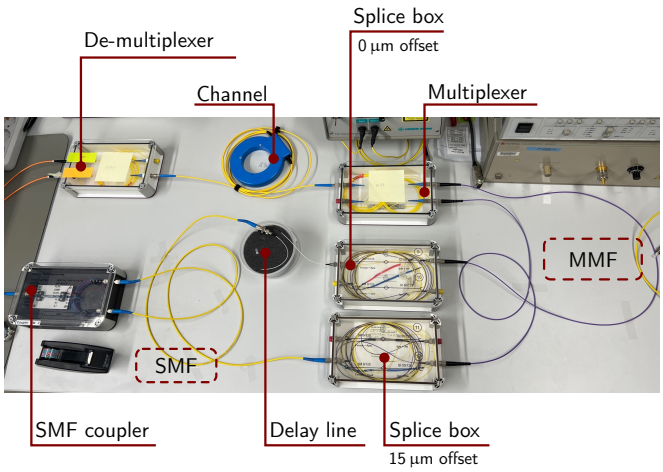

Figure 6. Experimental measurement setup with the PFS configuration using a 167.27 m delay line and an MMF channel.

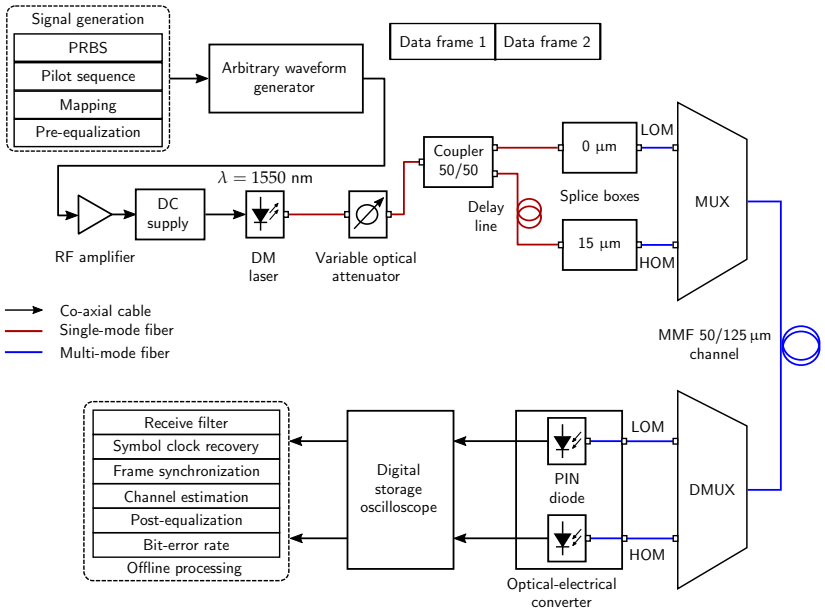

Figure 7. Experimental setup for the joint-PPE scheme by using an optical (2×2) MIMO system with an MMF channel with a PFS configuration.

The design of the post-equalizer is based on the concept of the MMSE equalizer. It implies that the counterbalance between noise enhancement and ISI mitigation is taken into account. It is worth noting that the sum of pre- and post-equalizer taps remains constant while comparing the joint-PPE with the PE-only. While considering the cost-effectiveness and complexity of the experimental setup, a PFS configuration using the delay lines is employed. The structure of this setup includes the concatenation of the two different data frames. By using a coupler and a delay line on one input, the concatenated data frames are segregated simply by delaying one of the input equivalent to the length of the data frame. The length of the delay line L_{d} is calculated as

$$L_{\mathrm{d}} = \frac{\mathrm{c} \cdot L_{\mathrm{m}}}{\eta_{\mathrm{core}} \cdot f_{\mathrm{T}}} \ , \tag{9}$$

where c is the speed of light, and L_{m} represents the data frame length. The refractive index of the core is η_{core} and f_{T} is the symbol rate. The analysis of delay lines with different pseudo-random binary sequence (PRBS) sequence lengths is provided in Table 2. In Figure 7, the transmitter includes the signal generation unit, where the two sequences are mapped either to the PAM-2 or to the PAM-4 constellations on all the layers. Additionally, the pilot symbols are appended with these sequences. The channel state information is computed using the least-square pilot estimator algorithm. The measured channel impulse response of an MMF channel at a symbol rate of 2.5 GHz on each layer is illustrated in Figure 3. It is clear from the plot of the estimated channel that a significant amount of cross-talk is present between $h_{12}[k]$ and $h_{21}[k]$. Moreover, the ISI is considerably high at $h_{11}[k]$ compared to $h_{22}[k]$. Therefore, the joint-PPE scheme aims to completely mitigate the ISI and ICI with a minimal increase in noise amplification.

Using the pre-equalizer, the multi-level signals with the calculated amplitudes are generated with the aid of the optimization algorithm. Afterwards, the data frames are concatenated with the help of an arbitrary wave generator, which operates at a symbol rate of 2.5 GHz on each layer. The radio-frequency (RF) amplifier with a gain of 20 dBm is included for better extinction ratios between the multi-level signals. The directly modulated laser (DML) source, with $P_s^{(\max)} = 1.1$ dBm and operating wavelength of $\lambda = 1550$ nm, modulates the electrical data signal. With the help of a single-mode coupler and a delay line of 167.27 m, the data frames are segregated and launched into the MMF with the light

launching conditions of 0 µm and 15 µm. In contrast to the setup with two different DMLs for two layers, the advantage of using the PFS setup is that both MIMO layers operate on an identical wavelength and the overall complexity is minimized. A variable optical attenuator (VOA) is incorporated in the setup for the purpose of BER performance evaluation over a distinct range of the average optical received powers. Please note that the power at both layers is constrained before transmission. The lower-order mode (LOM) groups are excited using the centric launching condition into the MMF and high-order mode (HOM) groups are generated with an eccentric launching condition of 15 µm. These transmitted signals are multiplexed together using a custom-made fusion coupler (labeled as MUX) and launched into a 100 m long MMF. After propagating through the MMF channel, the transmitted signal is severely degraded with ISI and ICI as the modal dispersion is considerably higher compared to the chromatic dispersion in the SMF-based optical system.

At the receiver's side, a de-multiplexer (DMUX) segregates the LOMs and HOMs. Eventually, the MMF photo-detector, labeled as a PIN diode, converts the optical signals into the electrical domain. These signals are further amplified using a trans-impedance amplifier. The large sensing areas of the PIN diodes lead to an inherent increase in capacitance. Finally, the electrical signals are captured by the digital storage oscilloscope (DSO), which are stored with 40 GSa/s and a bandwidth of 13.6 GHz. In the end, the stored signals are forwarded to the offline signal processing chain using one sample per symbol. The receive filtering is the first step, which is adapted according to the rectangular transmit filter with a similar impulse response. This step is followed by the symbol clock recovery, frame synchronization and channel estimation. Initially, an MMSE post-equalizer is employed. Afterwards, the post-equalizer is replaced by the joint-PPE filter. In the end, the BER performance is measured with respect to the average optical received power P_r. For maintaining the reliability of the results, 52 frames consisting of over a million bits on each layer are evaluated. Moreover, the results do not consider the forward error correction decoding.

The BER in dependence on the average optical received power P_r is demonstrated in Figure 8, where the two scenarios with different modulation formats are shown. The corresponding results are presented in a tabular form, where the optical received power gains are demonstrated at a BER of 10^{-4} in Table 3. Evidently, the required optical received power is reduced when the joint-PPE scheme is employed as compared to PE-only. While using PAM-2 with a jointly computed 4-taps pre-equalizer and 21-taps MMSE post-equalizer, a P_r gain of ≈1.93 dB is achieved in comparison to a PE-only. Correspondingly, when the PAM-4 format is used on both the MIMO inputs with the proposed joint-PPE filter, the P_r gains of ≈0.96 dB and ≈1.84 dB are noted incorporating the two and four taps pre-equalizer, respectively. When the joint-PPE scheme with the PAM-4 MIMO inputs is analyzed, the ΔP_r gain of ≈0.88 dB with different pre-equalizer lengths is observed. It implies that the joint-PPE scheme with $L_\mathrm{p} = 2$ should be preferred to limit the complexity of the system as it provides similar performance benefits as the joint-PPE scheme with $L_\mathrm{p} = 4$. In summary, the experimental results confirm the hypothesis, which states the usefulness of the joint-PPE over the PE-only. The results prove that the interferences such as ISI and ICI are completely compensated with a minimal noise amplification, which are highlighted by the improvements in the BER performance. The eye diagrams of the received electrical signals $y_\nu(t)$ with PAM-4 and PAM-2 transmissions are represented in Figure 9 and Figure 10, respectively. It is clear from the wider eye openings that the

Table 2. Analysis of the required length of the delay lines for the PFS configuration.

PRBS Length	Symbol Rate (in GHz)	Delay Time (in ns)	Delay Length (in m)
512	2.5	204.8	41.82
1024	2.5	409.6	83.64
2048	2.5	819.2	167.27
4096	2.5	1600	334.55

transmission quality is enhanced when the proposed joint-PPE scheme with $L_p = 4$ is utilized over MMSE PE-only.

Table 3. Measured optical received power P_r gain of the (2×2) optical MIMO system at 10^{-4} BER using a 100 m long MMF channel at $f_T = 2.5$ GHz.

Scenario	Modulation Format	Equalization	L_p	L_f	P_r (in dBm) at BER of 10^{-4}	P_r Gain (in dB)
First scenario	PAM-2	PE-only	-	25	−14	-
		Joint-PPE	2	23	−15.13	1.13
			4	21	−15.93	1.93
Second scenario	PAM-4	PE-only	-	25	−9.95	-
		Joint-PPE	2	23	−10.91	0.96
			4	21	−11.79	1.84

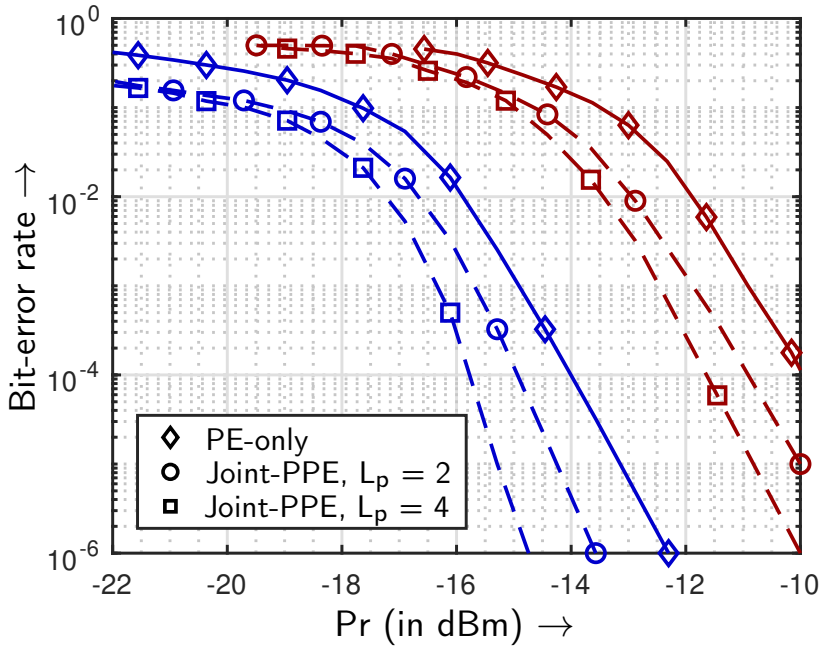

Figure 8. BER in dependence on the average optical received power while using a 100 m long MMF channel and MMSE equalizer, where PAM-2 and PAM-4 are depicted with blue and red color, respectively.

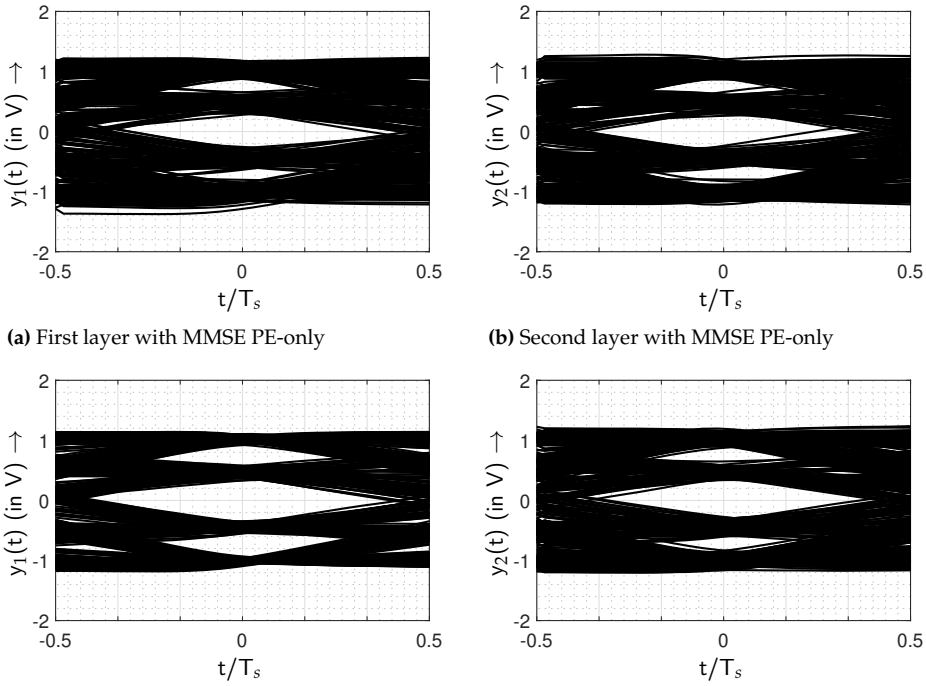

(a) First layer with MMSE PE-only **(b)** Second layer with MMSE PE-only

(c) First layer with joint-PPE using $L_{\mathrm{p}} = 4$ **(d)** Second layer with joint-PPE using $L_{\mathrm{p}} = 4$

Figure 9. Eye diagrams of the joint-PPE with $L_{\mathrm{p}} = 4$ compared with MMSE PE-only using PAM-4 transmission.

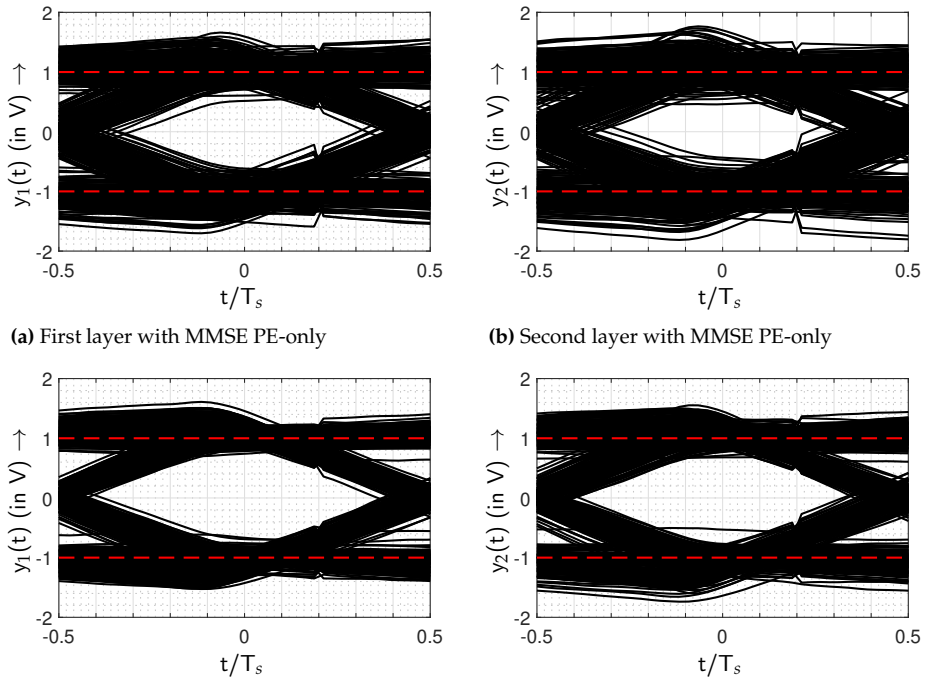

(a) First layer with MMSE PE-only **(b)** Second layer with MMSE PE-only

(c) First layer with joint-PPE using $L_{\mathrm{p}} = 4$ **(d)** Second layer with joint-PPE using $L_{\mathrm{p}} = 4$

Figure 10. Eye diagrams of the joint-PPE with $L_{\mathrm{p}} = 4$ compared with MMSE PE-only using PAM-2 transmission.

6. Conclusions

This work has proposed the joint-PPE scheme for an optical MIMO system operating with HOM formats. The aim of minimal complexity surge and cost-effectiveness is achieved by using IM/DD system based on an MMF transmission link with a few-tap pre-equalizer.

The joint-PPE filter coefficients are estimated and optimized using the maximum power constraint of the laser source. From the experimental results, the proposed joint-PPE is potentially proved to be advantageous despite the critical dispersion-induced impairments due to the MMF channel. The results of this work highlight that the use of joint-PPE is more beneficial than the equalization limited to the receiver's side only.

7. Discussion

The work aims to analyze the performance benefits of the proposed joint-PPE scheme while utilizing a (2×2) SDM-based optical MIMO system with PAM-4 and PAM-2 formats. The joint-PPE over MMSE PE-only achieves a ≈2 dB gain in the required optical received power P_r to reach a BER of 10^{-4}. Using the PFS configuration with PAM-2 transmission, a two-tap pre-equalizer yields a P_r gain of ≈0.8 dB at a BER of 10^{-3} compared to MMSE PE-only. This is contrary to the conventional configuration in which a two-tap pre-equalizer reaches a P_r gain of just ≈0.5 dB at a BER of 10^{-3}, even in the presence of minor mode coupling and higher transmission power per layer [17]. Although a substantial modal dispersion exists due to an MMF link in the PFS configuration, the proposed joint-PPE scheme improves the BER performance within the power and cost budgets. The calculation of joint-PPE coefficients requires an accurate channel estimation. During the experiments, the measured channel was very stable. However, external perturbations, such as wind and temperature, can influence channel characteristics [18,19]. Further research must focus on the feedback mechanism for continuously adapting the joint-PPE coefficients according to the dynamic channel environment.

Author Contributions: Conceptualization, J.S., A.A. and S.L.; methodology, J.S., A.A. and S.L.; software, J.S.; validation, A.A. and S.L.; formal analysis, J.S.; investigation, J.S.; resources, J.S., A.A. and S.L.; data curation, J.S.; writing—original draft preparation, J.S.; writing—review and editing, A.A. and S.L.; visualization, J.S.; supervision, A.A. and S.L.; project administration, A.A. and S.L. All authors have read and agreed to the published version of the manuscript.

Funding: This research received no external funding.

Institutional Review Board Statement: Not applicable.

Informed Consent Statement: Not applicable.

Data Availability Statement: The data that support the findings of this study are available on request from the corresponding author. The data are not publicly available due to privacy or ethical restrictions.

Conflicts of Interest: The authors declare no conflict of interest.

References

1. Zhu, Z.; Chen, J.; Zhao, M.; Pang, F.; Zhang, Q.; Ye, N. IM/DD mode division multiplexing transmission enabled by machine learning-based linear and nonlinear MIMO equalization. *Opt. Commun.* **2021**, *488*, 126832. [CrossRef]
2. Greenberg, M.; Nazarathy, M.; Orenstein, M. Data parallelization by optical MIMO transmission over multimode fiber with intermodal coupling. *J. Light. Technol.* **2007**, *25*, 1503–1514. [CrossRef]
3. Agarwal, G.P. *Fiber-Optics Communication Systems*; John Wiley & Sons: Hoboken, NJ, USA, 2012; Volume 222.
4. Lei, Y.; Li, J.; Fan, Y.; Yu, D.; Fu, S.; Yin, F.; Dai, Y.; Xu, K. Space-division-multiplexed transmission of 3 × 3 multiple-input multiple-output wireless signals over conventional graded-index multimode fiber. *Opt. Express* **2016**, *24*, 28372–28382. [CrossRef] [PubMed]
5. Lei, Y.; Li, J.; Meng, Z.; Wu, R.; Wan, Z.; Fan, Y.; Zhang, W.; Yin, F.; Dai, Y.; Xu, K. Feasibility of space-division-multiplexed transmission of ieee 802.11 n/ac-compliant wireless mimo signals over om3 multimode fiber. *J. Light. Technol.* **2018**, *36*, 2076–2082. [CrossRef]
6. Velázquez-Benítez, A.M.; Antonio-López, J.E.; Alvarado-Zacarías, J.C.; Fontaine, N.K.; Ryf, R.; Chen, H.; Hernández-Cordero, J.; Sillard, P.; Okonkwo, C.; Leon-Saval, S.G.; et al. Scaling photonic lanterns for space-division multiplexing. *Sci. Rep.* **2018**, *8*, 8897. [CrossRef] [PubMed]
7. Durst, M.E.; Kobat, D.; Xu, C. Tunable dispersion compensation by a rotating cylindrical lens. *Opt. Lett.* **2009**, *34*, 1195. [CrossRef] [PubMed]

8. Iijima, Y.; Yuminaka, Y. Double-rate equalization using Tomlinson-Harashima precoding for multi-valued data transmission. In Proceedings of the IEEE 46th International Symposium on Multiple-Valued Logic (ISMVL), Sapporo, Japan, 18–20 May 2016; pp. 66–71.
9. Rajbhandari, S.; Chun, H.; Faulkner, G.; Haas, H.; Xie, E.; McKendry, J.J.D.; Herrnsdorf, J.; Gu, E.; Dawson, M.D.; O'Brien, D. Neural network-based joint spatial and temporal equalization for MIMO-VLC System. *IEEE Photonics Technol. Lett.* **2019**, *31*, 821–824. [CrossRef]
10. Yuksekkaya, B.; Toker, C. A general joint transceiver sesign for multiuser MIMO channel equalization. In Proceedings of the IEEE 72nd Vehicular Technology Conference—Fall (VTC), Ottawa, ON, Canada, 6–9 September 2010; pp. 1–5.
11. Tang, X.; Qiao, Y.; Chen, Y.W.; Lu, Y.; Chang, G.K. Digital Pre- and Post-Equalization for C-Band 112-Gb/s PAM4 Short-Reach Transport Systems. *J. Light. Technol.* **2020**, *38*, 4683–4690. [CrossRef]
12. Wan, Z.; Li, J.; Shu, L.; Fu, S.; Fan, Y.; Yin, F.; Zhou, Y.; Dai, Y.; Xu, K. 64-Gb/s SSB-PAM4 transmission over 120-km dispersion-uncompensated SSMF With blind nonlinear equalization, adaptive noise-whitening postfilter and MLSD. *J. Light. Technol.* **2017**, *35*, 5193–5200. [CrossRef]
13. Zou, D.; Chen, Y.; Li, F.; Li, Z.; Sun, Y.; Ding, L.; Li, J.; Yi, X.; Li, L.; Li, Z. Comparison of Bit-Loading DMT and Pre-Equalized DFT-Spread DMT for 2-km Optical Interconnect System. *J. Light. Technol.* **2019**, *37*, 2194–2200. [CrossRef]
14. Ahrens, A.; Pankow, J.; Aust, S.; Lochmann, S. Optical MIMO multimode fiber links—Channel measurements and system performance analysis. In Proceedings of the International Conference on Data Communication Networking and International Conference on Optical Communication Systems, Seville, Spain, 18–21 July 2011; pp. 128–132
15. Pankow, J.; Aust, S.; Lochmann, S.; Ahrens, A. Modulation-mode assignment in SVD-assisted optical MIMO multimode fiber links. In Proceedings of the 15th International Conference on Optical Network Design and Modeling (ONDM), Bologna, Italy, 8–10 February 2011; pp. 1–6
16. Waltz, R.; Morales, J.; Nocedal, J.; Orban, D. An interior algorithm for nonlinear optimization that combines line search and trust region steps. *Math. Program.* **2005**, *107*, 391–408 [CrossRef]
17. Singh, J.; Gotten, M.; Ahrens, A.; Lochmann, S. Joint pre- and post-equalization in optical MIMO systems using multi-level signaling. In Proceedings of the 2022 IEEE 95th Vehicular Technology Conference: (VTC2022-Spring), Helsinki, Finland, 19–22 June 2022.
18. Choutagunta, K.; Roberts, I.; Kahn, J.M. Efficient quantification and simulation of modal dynamics in multimode fiber links. *J. Light. Technol.* **2019**, *37*, 1813–1825. [CrossRef]
19. Lei, Y.; Lu, Q.; Chen, B.; Guo, Z. Channel condition and outage performance of mode-division-multiplexing enabled MIMO system with zero-forcing receiver. *IEEE Commun. Lett.* **2022**, *26*, 2390–2394. [CrossRef]